RSC Advances

PAPER

View Article Online
View Journal | View Issue

Cite this: *RSC Adv.*, 2016, **6**, 113826

# Microporous organic polymers based on tetraethynyl building blocks with *N*-functionalized pore surfaces: synthesis, porosity and carbon dioxide sorption†

Hongjiang Zhang,[a] Chong Zhang,[b] Xunchang Wang,[a] Zexiong Qiu,[c] Xinmiao Liang,[d] Bing Chen,[d] Jiawei Xu,[a] Jia-Xing Jiang,*[b] Yuda Li,[a] Hui Li[a] and Feng Wang*[a]

Received 17th August 2016
Accepted 15th November 2016

DOI: 10.1039/c6ra20765k

www.rsc.org/advances

A series of microporous organic polymers (MOPs) based on tetraethynyl monomers such as tetrakis(4-ethynylphenyl)methane and tetrakis(4-ethynylphenyl)silane was synthesized *via* conventional Sonogashira–Hagihara coupling reaction. The resulting MOPs were characterized by thermogravimetric analyses, IR-spectra, scanning electron microscopies, and the Brunauer–Emmett–Teller (BET) method. The incorporation of triphenylamine or azobenzene moieties into the polymer skeleton increases the number of electron donating basic nitrogen sites in the porous frameworks. Thus, these MOPs could exhibit efficient adsorption of Lewis acidic $CO_2$ molecules and display good $CO_2$-over-$N_2$ selectivity. The triphenylamine-based polymer, TEPM-TPA, shows a high BET specific surface area up to 1072 $m^2\ g^{-1}$ with a moderate $CO_2$ uptake capacity of 2.41 mmol $g^{-1}$ at 273 K and 1.13 bar. As for separation of $CO_2$, both TEPM-Azo and TEPS-Azo exhibit relatively high $CO_2$-over-$N_2$ selectivities of 70.8 and 64.7 at 273 K, respectively, due to the $N_2$-phobic feature of azo-based polymers.

## Introduction

In recent years, global warming has become a major issue in climate change.[1] Overwhelming scientific consensus has correlated global warming to anthropogenic $CO_2$ emission. Thus, one of the promising technologies to protect the environment is to develop new efficient adsorbents for $CO_2$ capture and storage (CCS).[2] Traditional $CO_2$ capture is based on the chemical adsorption of $CO_2$ using amine-containing solvents.[3] However, because of high energy consumption, solvent regeneration, and the corrosion of the equipment, scientists are seeking new materials for CCS.

Microporous organic polymers (MOPs) have drawn much attention due to their promising applications such as gas separation matrices,[4–6] heterogeneous catalysis,[7–10] supercapacitors,[11–13] and sensing materials.[14–16] MOPs generally possess large surface area, excellent chemical and thermal stability, tunable pore properties, low skeleton density, and synthetic diversity.[6] These features could make MOPs became strong candidates for post-combustion CCS, and they have been the subject of recent research interests.[4,17–29] The surface modification of MOPs is an effective approach to modulate framework–$CO_2$ interactions. It has been proved that the introduction of nitrogen functionalities into the backbone of MOPs could enhance $CO_2$ and energy storage properties owing to Lewis-acid–Lewis-base electrostatic interactions of the nitrogen atoms with $CO_2$ molecules.[17,20–23,30–34] Therefore, synthesis of new MOPs using nitrogen-rich monomers has attracted considerable scientific interest in recent years. A range of MOPs have been successfully developed for CCS applications based on various nitrogen-containing building blocks, such as covalent triazine frameworks,[30–32] benzimidazole-linked polymers,[33,34] carbazole-based MOPs,[20,23] and triphenylamine-containing polymers.[21] A recent study by Patel and coworkers has shown that nitrogen–nitrogen double bonds (azo-bond) in the porous polymer main chain can play important roles in $CO_2$ storage and separation application.[35] These new azo-functionalized MOPs demonstrated that the π-conjugated azo-bond could act as an electron donor, and thus enhance host–guest interactions.[35–37]

Cooper and coworkers applied Sonogashira–Hagihara coupling chemistry to prepare a series of MOPs with controllable pore dimensions and surface areas by varying building blocks.[38]

---

[a] *Key Laboratory for Green Chemical Process of Ministry of Education, School of Chemical Engineering and Pharmacy, Wuhan Institute of Technology, Wuhan 430073, P. R. China. E-mail: psfwang@wit.edu.cn*

[b] *School of Materials Science and Engineering, Shaanxi Normal University, Xi'an 710062, P. R. China. E-mail: jiaxing@snnu.edu.cn*

[c] *School of Materials Science and Engineering, Wuhan University of Technology, Wuhan 430070, P. R. China*

[d] *State Key Laboratory of Magnetic Resonance and Atomic and Molecular Physics, Wuhan Institute of Physics and Mathematics, Chinese Academy of Science, Wuhan 430071, P. R. China*

† Electronic supplementary information (ESI) available. See DOI: 10.1039/c6ra20765k

Impressively, the use of tetraethynyl monomers such as tetrakis(4-ethynylphenyl)methane[28] and tetrakis(4-ethynylphenyl)silane[29] is prominent for the generation of 3D-porous assemblies. Their strong covalent linkage leads to high chemical and thermal stability. In this work, we have rationally designed and synthesized a series of nitrogen-rich MOPs by copolymerization of tetraethynyl monomers with tris(4-iodophenyl)amine or 4,4′-diiodoazobenzene *via* Sonogashira–Hagihara coupling reaction. The highly cross-linked porous structure can substantially increase the surface area of the resulting polymer networks and, on the other hand, the incorporation of azobenzene or triphenylamine groups from the building block into the polymer skeleton could enhance the binding affinity between the adsorbent and $CO_2$ molecules, and thus lead to the increase of $CO_2$ capture capacity. As we expected, azo-based polymers exhibited excellent $CO_2$ adsorption selectivity against $N_2$. This unique property of TEPM-Azo and TEPS-Azo, along with their chemical and thermal stability, makes them ideal candidates for post-combustion $CO_2$ separation.

## Experimental

### Materials

All the reagents, unless otherwise specified, were purchased from Sigma-Aldrich Co., Acros, and Tokyo Chemical Industry Co., Ltd. and were used without further purification. All the solvents were further purified under nitrogen flow. Tetrakis(4-ethynylphenyl)methane (1), tetrakis(4-ethynylphenyl)silane (2) and tris(4-iodophenyl)amine (3) were prepared according to the previously reported method.[28,29,39]

### Measurements

The NMR spectra were recorded on an Agilent 300-MR NMR spectrometer. Thermogravimetric analysis (TGA) was performed by a differential thermal analysis instrument (Q1000DSC + LNCS + FACSQ600SDT) over the temperature range from 30 to 1000 °C with a heating and cooling rate of 10 °C $min^{-1}$ under nitrogen. Solid state magic angle spinning $^{13}C$ CP/MAS NMR measurements were carried out on a Varian Infinity-Plus 300 MHz NMR spectrometer at a MAS rate of 10 kHz. The FT-IR spectra were collected in transmission on a Tensor 27 FT-IR spectrometer (Bruker) using KBr disks. The polymer morphology was achieved using a field-emission scanning electron microscopy (SEM) (JSM-7001F, JEOL, Tokyo, Japan). Powder X-ray diffraction measurement (PXRD) was carried out on an X-ray diffractometer (D/Max-3c). The measurements of the surface area and pore-size distributions (PSDs) of the samples were performed on an ASAP 2420-4 (Micromeritics) volumetric adsorption analyzer by means of nitrogen adsorption and desorption at 77.3 K. Samples were degassed at 120 °C for 15 h under vacuum ($10^{-5}$ bar) before analysis. The surface areas were calculated in the relative pressure ($P/P_0$) range from 0.05 to 0.20. PSDs and pore volumes were derived from the adsorption branches of the isotherms using the nonlocal density functional theory (NL-DFT). Gas sorption isotherms were measured on an ASAP 2420-4 as well.

### Synthesis

**4,4′-Diiodoazobenzene (4).** 4-Iodoaniline (6 g, 27.4 mmol), $KMnO_4$ (10.5 g, 6.26 mmol) and $CuSO_4 \cdot 5H_2O$ were added to a degassed solution of dichloromethane (160 mL) and stirred at room temperature for 3 days. The reaction mixture was filtered through Celite and the solvent was evaporated under reduced pressure. The crude product was purified on a silica gel column using a petroleum ether/dichloromethane (3 : 1 by volume) mixture as eluent. An orange solid of 4 was isolated in 15% yield (0.89 g). $^1H$ NMR (300 MHz, $CDCl_3$), $\delta$ (TMS, ppm): 7.84 (d, 4H), 7.61 (d, 4H).

### Polymerization

All of the polymer networks were synthesized by palladium-catalyzed Sonogashira–Hagihara cross-coupling polycondensation of arylethynylenes and aryl halides. The molar ratio of ethynyl to halogen functionalities in the monomer feed was set at 1.5 : 1 according to the reported procedure.[38] The purification of the polymers was conducted in air with yield of 80–90%. A typical procedure for TEPM-Azo is given below:

Tetrakis(4-ethynylphenyl)methane (81 mg, 0.195 mmol), 4,4′-diiodoazobenzene (113 mg, 0.26 mmol), tetrakis(triphenylphosphine)palladium(0) (15 mg), and copper(I) iodide (10 mg) were dissolved in a mixture of anhydrous DMF (5 mL) and triethylamine (5 mL). The reaction mixture was heated to 90 °C and stirred for 72 h under nitrogen atmosphere. The mixture was cooled to room temperature, and the precipitated polymer networks was filtered and washed four times with dichloromethane, water, methanol, and acetone to remove any unreacted monomer or catalyst residues. The product was dried in vacuum for 24 h at 100 °C. Yield: 80.1%. Apparent BET surface area: 564 $cm^3$ $g^{-1}$.

## Result and discussion

### Synthesis and characterization

The synthesis of 4,4′-diiodoazobenzene (monomer 4) is shown in Scheme 1. Starting from the commercially available 4-iodoaniline, 4,4′-diiodoazobenzene was prepared by the oxidative coupling of two equivalents of 4-iodoaniline in the presence of $CuSO_4 \cdot 5H_2O$ and $KMnO_4$ under nitrogen atmosphere in dichloromethane.[40] The polymer networks in this study were synthesized by palladium-catalyzed Sonogashira–Hagihara coupling polycondensation. The polymerization reactions were performed at a fixed reaction temperature (90 °C) and the reaction time (72 h). The molar ratio of ethynyl to iodine functionalities in the monomer feed was fixed at 1.5 : 1 since maximum surface areas was observed at this ratio based on the previous reports.[38] The general synthetic routes to the polymer networks are shown in Scheme 1. The polymer networks are insoluble in common organic solvents due to their highly cross-linked structures and the rigid skeleton. The FT-IR spectra revealed no residual trace of the specific vibration bands related to terminal alkynes at around 3280 $cm^{-1}$,[28] therefore suggesting high conversion of the starting monomers (Fig. S1†). The $^{13}C$ solid-state NMR (CP/MAS) measurements were carried out to

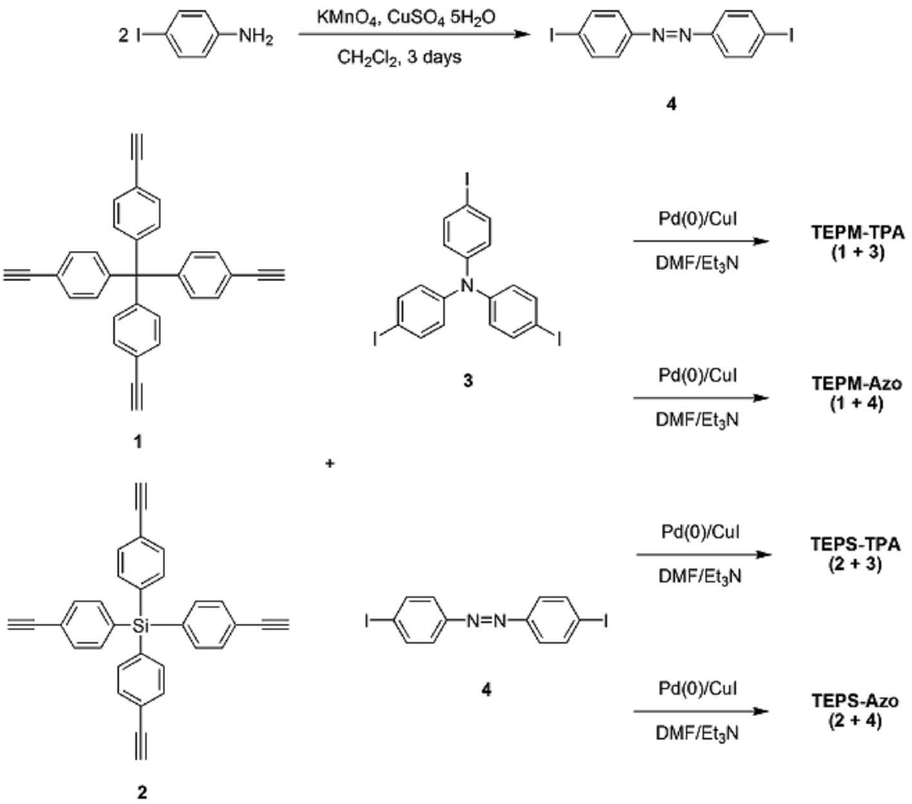

Scheme 1 Synthetic routes to 4,4′-diiodoazobenzene (4) and the polymer networks.

study the local structures of these polymers (Fig. S2†). All of the carbon signals with a chemical shift exceeding 110 ppm are related to aromatic carbon atoms of the building phenylene groups in the framework. The peak at around 91 ppm in the NMR spectra is assigned to the sp carbons in alkyne bonds, thus suggesting that this cross-coupling reaction is effective for the synthesis of these polymer networks.[41,42] A well-resolved peak is detected at 65 ppm associated with the quaternary carbon atom in tetrakis(4-ethynylphenyl)methane, indicating that tetrakis(4-ethynylphenyl)methane is the main building units in the polymer networks TEPM-TPA and TEPM-Azo.[41,42] Additionally, the azo-linkage formation was further confirmed by the presence of characteristic signals for the –C–N=N–C– bond at around 152 ppm in NMR spectra of azo-based polymers.[35] TGA measurements were carried out to evaluate the thermal stability of these polymers (Fig. S3†). All the polymer networks exhibit good stability, showing less than 5% weight loss at around 480 °C under nitrogen flow. Powder X-ray diffraction measurements suggested that all the polymer networks are amorphous solid in nature (Fig. S4†). The SEM images of the obtained polymer networks are shown in Fig. 1. For the polymer networks, similar morphology can be observed to be solid submicrometer particles with different size range from 10 to 100 nm.

### Porosity measurements

In order to study the porosity of these polymer networks, sorption analysis using nitrogen as the sorbent molecules was carried out. Nitrogen adsorption/desorption isotherms of these materials measured at 77.3 K are shown in Fig. 2a. The polymer networks exhibited Type I isotherms with a steep nitrogen gas uptake at low pressure according to the International Union of Pure and Applied Chemistry (IUPAC) classification, suggesting that micropores are dominant in these polymer networks.[18] The gradual increase in $N_2$ uptake ($P/P_0 = 0.05–0.9$) at 77.3 K is due to the presence of mesopores in the polymers. The significant hysteresis between adsorption and desorption was observed in the isotherms for all the polymer networks in the whole range of relative pressure, which is in agreement with the fact that all the MOPs contain both meso- and microporosity. As shown in

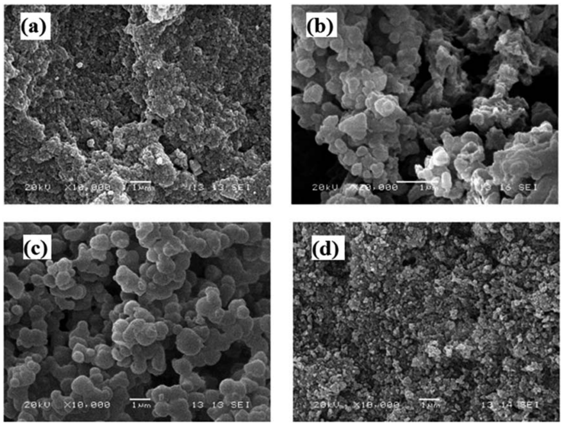

Fig. 1 SEM images of TEPM-TPA (a), TEPM-Azo (b), TEPS-TPA (c), TEPS-Azo (d), scale bars: 1 μm.

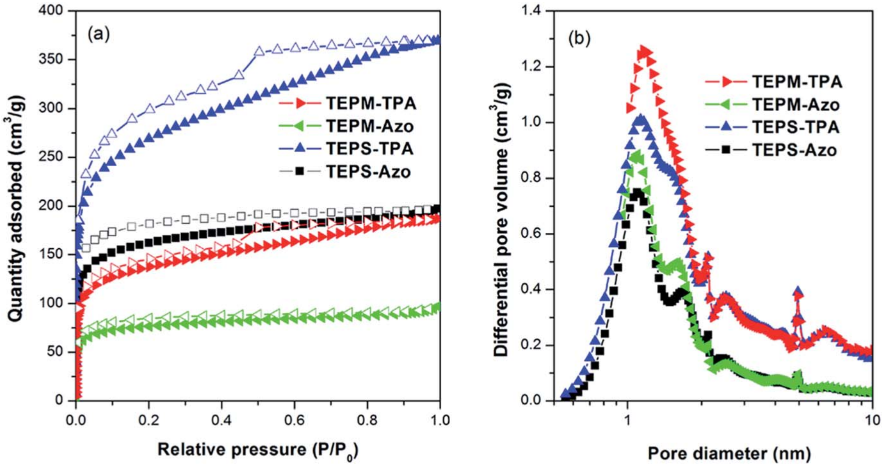

Fig. 2 (a) Nitrogen adsorption/desorption isotherms (the adsorption branch is labeled with filled symbols and desorption branch is labeled with open symbols); (b) pore size distribution curves calculated by NL-DFT for the polymer networks.

Fig. 2b, similar PSD profiles based on the adsorption branch of the isotherm using nonlocal density functional theory (NL-DFT) were found for the obtained polymer TEPM-TPA and TEPS-TPA. Both polymers show abundant micropore structures with micropore diameters centered at around 1.1 nm. As for the polymer TEPM-Azo and TEPS-Azo, the PSDs are relative broader in the range of 1.1–2.1 nm compared with those of TEPM-TPA and TEPS-TPA, indicating that much more mesopores and/or macropores in these two polymers. Besides, TEPM-Azo and TEPS-Azo show a spot mesopores peaks at around 5 nm. The PSD curves of the polymer networks are in good agreement with the shape of the nitrogen isotherms (Fig. 2a) and suggest that the pores of the polymer networks are dominated by micropores. The contribution of microporosity to the networks can be calculated as the ratio of the micropore volume over the total pore volume. As shown in Table 1, the ratios indicated that polymer networks TEPM-TPA, TEPS-TPA, TEPM-Azo, and TEPS-Azo possess a ratio of 0.63, 0.74, 0.79, and 0.90, respectively. The BET specific surface areas of TEPM-TPA and TEPS-TPA are 1072 and 937 m$^2$ g$^{-1}$, respectively, which are higher than those of TEPS-Azo (564 m$^2$ g$^{-1}$) and TEPM-Azo (598 m$^2$ g$^{-1}$) containing the azobenzene building block. It should be noted that TEPM-TPA and TEPS-TPA exhibit comparable surface area to the most of reported conjugated microporous poly(aryleneethynylene) (PAE) networks by Sonogashira–Hagihara cross-coupling chemistry.[26]

## Gas uptake of CO$_2$, H$_2$, and CH$_4$

Because of the considerable porosity and nitrogen-rich features, we were interested in assessing their performance in gas uptake. The CO$_2$ uptake of the polymer networks were measured up to 1.13 bar at 273, 283, and 298 K, respectively (Fig. 3a and b, S5,† and Table 2). It can be seen that the CO$_2$ uptake capacity enhances monotonically with increasing CO$_2$ pressure. TEPM-TPA exhibited the highest CO$_2$ uptake at both 273 and 298 K, adsorbing 2.41 and 1.39 mmol g$^{-1}$ at 1.13 bar among the resulting four polymers. When azobenzene is copolymerized with tetrakis(4-ethynylphenyl)methane, the absolute CO$_2$ uptake capacity of the polymer decreases from 2.41 mmol g$^{-1}$ for TEPM-TPA to 1.78 mmol g$^{-1}$ for TEPM-Azo. This could be explained by the decrease of surface area and pore volume for the polymer networks as mentioned above (Table 1). The CO$_2$ uptake of 2.41 mmol g$^{-1}$ for TEPM-TPA is comparable to that of many reported MOPs produced by Sonogashira–Hagihara coupling reaction at the same conditions, such as the conjugated microporous PAE networks without nitrogen-containing building blocks and their metalized derivatives,[41,43–47] tetraphenylmethane-based hypercrosslinked porous aromatic frameworks (2.27 mmol g$^{-1}$ for PAF-32-OH),[48] the tri(4-ethynylphenyl)amine-based porous aromatic frameworks (1.19–2.50 mmol g$^{-1}$),[42] the triazine-functionalized CMPs (2.62 mmol g$^{-1}$ for TNCMP-2),[49] the phenolsulfonephthalein-containing CMPs (2.77 mmol g$^{-1}$ for BFCMP-2),[50] but still lower than that of other tetrakis(4-ethynylphenyl)methane-based MOPs (3.77 mmol g$^{-1}$, 5.07 mmol g$^{-1}$, and 4.28 mmol g$^{-1}$ for F-MOP-1, F-MOP-2, and HEX-POP-3, respectively),[51,52] the imine-linked porous polymer frameworks (*e.g.* 6.1 mmol g$^{-1}$ for PPF-1),[53] the benzimidazole-incorporated porous polymer

Table 1 Summary of pore properties for the polymer networks

| Polymer | $S_{\text{BET}}$[a] (m$^2$ g$^{-1}$) | $S_{\text{Micro}}$[b] (m$^2$ g$^{-1}$) | $V_{\text{Micro}}$[c] (cm$^3$ g$^{-1}$) | $V_{\text{Total}}$[d] (cm$^3$ g$^{-1}$) | $S_{\text{Micro}}$/$S_{\text{BET}}$ (%) | $V_{\text{Micro}}$/$V_{\text{Total}}$ (%) |
|---|---|---|---|---|---|---|
| TEPM-TPA | 1072 | 901 | 0.446 | 0.708 | 84.05 | 62.99 |
| TEPM-Azo | 598 | 552 | 0.267 | 0.338 | 92.3 | 78.99 |
| TEPS-TPA | 937 | 787 | 0.396 | 0.536 | 83.99 | 73.88 |
| TEPS-Azo | 564 | 489 | 0.236 | 0.261 | 86.7 | 90.42 |

[a] Surface area calculated from N$_2$ adsorption isotherm in the relative pressure ($P/P_0$) range from 0.05 to 0.20. [b] Micropore surface area calculated from the N$_2$ adsorption isotherm using the *t*-plot method based on the Harkins–Jura equation. [c] The micropore volume derived from the *t*-plot method. [d] Total pore volume at $P/P_0 = 0.988$.

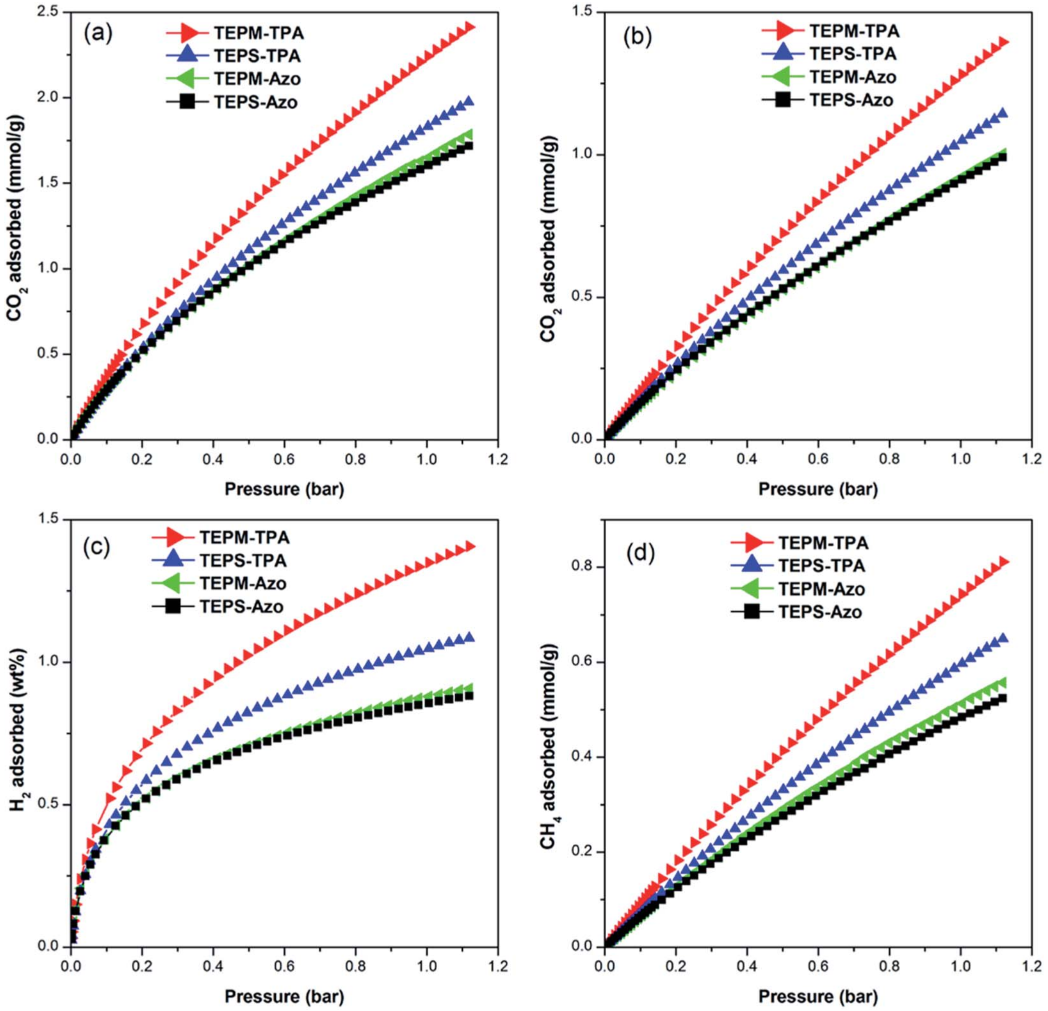

Fig. 3 (a) $CO_2$ adsorption isotherms collected at 273 K up to 1.13 bar for the polymer networks; (b) $CO_2$ adsorption isotherms collected at 298 K; (c) volumetric $H_2$ sorption curves collected at 77.3 K; (d) $CH_4$ adsorption isotherms collected at 273 K.

network of PPN-101 (5.1 mmol $g^{-1}$),[54] the microporous polycarbazole of CPOP-1 (4.8 mmol $g^{-1}$),[55] and the nanoporous azo-linked polymer of ALP-1 (5.36 mmol $g^{-1}$).[36] To determine the binding affinity between the polymer network and $CO_2$ molecules, the isosteric heats of adsorption ($Q_{st}$) were calculated from the $CO_2$ adsorption isotherms at 273, 283, and 298 K by using the Clausius–Clapeyron equation. As illustrated in Fig. 4, the $Q_{st}$ values of the obtained MOPs are in the range from 22 to 33 kJ $mol^{-1}$ at the near zero coverage. TEPM-Azo shows the highest $Q_{st}$ of 33 kJ $mol^{-1}$ among the polymers, which could be attributed to the high nitrogen content from azo groups in the skeleton of MOPs leading to a strong induce-dipole force with $CO_2$ molecules.[35–37] TEPS-Azo shows somewhat lower $Q_{st}$ values than TEPM-Azo. We suspect that even though the azo framework is same in both, TEPS-Azo with tetrakis(4-ethynylphenyl)silane units in the structure generated diminish basicity in the nitrogen species compared with those in TEPM-Azo with no Si (silicon is acidic in nature).[56] As for triphenylamine-containing polymers, the $Q_{st}$ value of TEPS-TPA is lower than that of TEPM-TPA, which is further support the above results in the case of azo-based polymers.

$H_2$ and $CH_4$ are important potential clean fuels for automotive technology; therefore, we also investigated the uptake capacities of these two gases by volumetric methods. The hydrogen sorption performance for the polymers networks was measured at 77.3 K up to a pressure of 1.13 bar. All adsorption

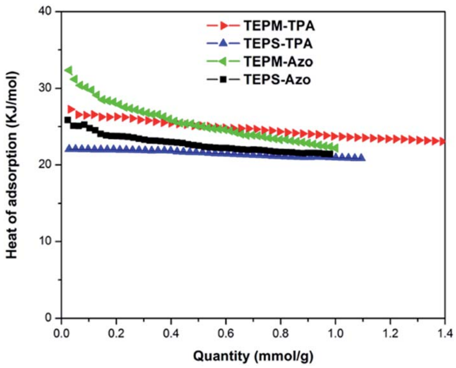

Fig. 4 Isosteric heats of adsorption for $CO_2$ calculated from the adsorption isotherms collected at 273, 283, and 298 K.

Table 2 Summary of gas uptakes values for the polymer networks

| Polymer | $H_2$ uptake[a] (wt%) | $CH_4$ uptake[b] (mmol $g^{-1}$) | $CO_2$ uptake[b] (mmol $g^{-1}$) | $CO_2$ uptake[c] (mmol $g^{-1}$) | Henry law selectivity[d] $CO_2/N_2$ | Henry law selectivity[d] $CO_2/CH_4$ | IAST selectivity[e] $CO_2/N_2$ | IAST selectivity[e] $CO_2/CH_4$ |
|---|---|---|---|---|---|---|---|---|
| TEPM-TPA | 1.4 | 0.81 | 2.41 | 1.39 | 26.3 | 4.6 | 36.9 | 5.1 |
| TEPM-Azo | 0.91 | 0.55 | 1.78 | 1 | 70.8 | 4.6 | 121.1 | 6.3 |
| TEPS-TPA | 1.08 | 0.65 | 1.97 | 1.14 | 20.5 | 3.9 | 30.5 | 4.9 |
| TEPS-Azo | 0.88 | 0.52 | 1.71 | 0.99 | 64.7 | 4.3 | 111.9 | 6.5 |

[a] Data collected by volumetric $H_2$ sorption method at 77.3 K and 1.13 bar. [b] Data collected at 273 K and 1.13 bar. [c] Data collected at 298 K and 1.13 bar. [d] Adsorption selectivity based on the Henry's law. [e] Calculated from ideal adsorbed solution theory (IAST) by using the $CO_2$, $N_2$, and $CH_4$ adsorption isotherms collected at 273 K.

isotherms show a gradual rise and reached a maximum of 0.88–1.4 wt% for hydrogen uptake (Fig. 3c). The $H_2$ uptake sorption properties of polymer networks can be correlated with the micropore volume and micropore surface area, which was also observed in other MOPs. Triphenylamine-based polymer networks exhibit higher $H_2$ adsorption capacity than azo-based polymer networks under the same conditions because of their lager surface areas and narrower pore sizes. The $CH_4$ uptakes at 273 K up to 1.13 bar (Fig. 3d) were also conducted. As expected, TEPM-TPA having the highest micropore volume and highest surface area shows the largest $CH_4$ uptake of 0.81 mmol $g^{-1}$.

### Selective $CO_2$ capture over $N_2$ and $CH_4$

We also investigated the $CO_2$ sorption selectivity over $N_2$ and $CH_4$ to assess their potential application in gas separation. The $CO_2$, $N_2$, and $CH_4$ adsorption isotherms were measured at 273 K up to 1.13 bar (Fig. S6†). The selectivity of the polymer networks was estimated using the ratios of the Henry's law constant calculated from the initial slopes of the single-component gas adsorption isotherms collected at 273 K at low pressure coverage less than 0.15 bar, which is typical partial pressure of $CO_2$ in flue gas. As shown in Table 2, TEPM-Azo and TEPS-Azo exhibit relative high $CO_2/N_2$ selectivity ratios of 70.8 and 64.7 at 273 K, whereas TEPM-TPA and TEPS-TPA show poor selectivities of 26.3 and 20.5, respectively. These results suggested that the azo-based polymer is efficient for $CO_2/N_2$ separation as expected because of the "$N_2$-phobicity" of the azo-linkage.[35–37] The differences in $CO_2/N_2$ selectivity between azo- and triphenylamine-based polymer networks indicate that in addition to the function of the surface area and pore size, the linkage is very important factor that affect $CO_2$ uptake and the $CO_2/N_2$ selectivity. The calculated $CO_2/N_2$ selectivities by both TEPM-Azo and TEPS-Azo are significantly higher than those of TEPM-TPA, TEPS-TPA, and some other MOPs such as tetraethynylspirobifluorene-based porous organic polymers POP (6.7–11.8 at 298 K),[57] porous hypercrosslinked aromatic polymers (PHAPs) using tetrahedral precursors (29.3–34.2 at 273 K),[56] tetraphenylsilane-containing porous covalent triazine polymer networks PCTP-2 (31.6 at 298 K),[58] tetra(4-(*N*-carbazolyl)phenyl)silane-based polycarbazole microporous polymer P-TCzPhSi (24.8 at 273 K),[59] the nanoporous azo-bridged polymers (30–43 at 273 K),[36] the carbazolic porous organic frameworks (19–37 at 273 K),[60] the imine-linked porous polymer frameworks (14.5–20.4 at 273 K),[53] the triazine-functionalized CMPs (9.0–25.2 at 298 K),[49] and the amide-functionalized CMPs (8.5–12 at 298 K) under the similar conditions.[61] Moreover, they are also comparable to the best azo-polymers ever reported like azo-COPs,[37] tri(4-ethynylphenyl) amine-containing polymers (72 and 63.9 for PAF-34 and PAF-34-OH, respectively),[42] tetrakis(4-ethynylphenyl)methane-based porous aromatic frameworks PAF-18-OH, PAF-26-COOH, and their metalized derivatives (16–73 at 298 K).[41,46] As for separation of $CH_4$, the calculated $CO_2/CH_4$ adsorption selectivity was about from 3.9 to 4.6 for the four polymers at 273 K. The results are comparable to that of most other reported porous organic polymers, such as tetrakis(4-ethynylphenyl)methane-based porous materials PAF-26 (4–9 at 298 K),[41] tetraethynylspirobifluorene-containing porous organic polymers POP (3.4–4.8 at 298 K),[57] the carbazole-based microporous organic polymer of Cz-POF (4.4–7.1 at 273 K),[60] the nanoporous covalent triazine-based frameworks (5–7 at 273 K),[62] the tetra-armed triphenylamine-containing MOPs (3.5–4.3 at 273 K),[63] and the azo-containing polymer networks ALP (8 at 273 K)[36] under the same conditions. The $CO_2/CH_4$ selectivity of the resultant polymers is considerably lower than that of $CO_2/N_2$ because of the higher polarizability of $CH_4$ than that of $N_2$.[60]

In addition, the gas adsorption selectivity for mixtures of $CO_2 : N_2$ (0.15 : 0.85) and $CO_2 : CH_4$ (0.05 : 0.95) were predicted by using ideal adsorbed solution theory (IAST) at a standardized temperature of 273 K. The method allows for the determination of the selectivities as a function of pressure, and has been widely used to predict binary gas mixture adsorption behaviors in many MOPs.[64,65] The adsorption data in Table 2 exhibit that the calculated IAST selectivities are higher than the values obtained from Henry's constant ratios, as observed for most reported porous materials.[17,30,31]

## Conclusions

In summary, we have synthesized a series of microporous organic polymer networks by using Sonogashira–Hagihara cross-coupling chemistry from two kinds of tetrahedral-shaped monomers of tetrakis(4-ethynylphenyl)methane and tetrakis(4-ethynylphenyl)silane. The resulting polymer networks incorporated nitrogen-rich triphenylamine or azobenzene groups present a high affinity to $CO_2$ molecules, which has been significantly verified by gas adsorption measurements. TEPM-TPA shows high BET specific surface area up to 1072 $m^2$ $g^{-1}$

with a moderate $CO_2$ uptake capacity of 2.41 mmol $g^{-1}$ at 273 K and 1.13 bar, which reinforce the benefits of tetrahedral monomers for the construction of high surface area materials. In addition, TEPM-Azo and TEPS-Azo exhibit relative high $CO_2/N_2$ selectivity of 70.8 and 64.7 at 273 K, respectively, which compared to that of some other reported polymer networks.

## Acknowledgements

This work was supported by Natural Science Foundation of China (Grant No. 51103111, 21304055 and 21574077), Education Ministry of China (Program for NCET-12-0714), Shaanxi Innovative Team of Key Science and Technology (2013KCT-17), the Fundamental Research Funds for the Central Universities (GK201501002), the Scientific Research Foundation for the Returned Overseas Chinese Scholars, the Open Fund of the State Key Laboratory of Luminescent Materials and Devices (2014-skllmd-11), and Graduate Innovative Fund of Wuhan Institute of Technology (Grant No. CX2014017, CX2014026).

## Notes and references

1 J. A. Logan, J. Regniere and J. A. Powell, *Front. Ecol. Environ.*, 2003, **1**, 130–137.
2 T. C. Drage, C. E. Snape, L. A. Stevens, J. Wood, J. Wang, A. I. Cooper, R. Dawson, X. Guo, C. Satterley and R. Irons, *J. Mater. Chem.*, 2012, **22**, 2815–2823.
3 F. Li and L. S. Fan, *Energy Environ. Sci.*, 2008, **1**, 248–267.
4 S. Ding and W. Wang, *Chem. Soc. Rev.*, 2013, **42**, 548–568.
5 S. Xu, Y. Luo and B. Tan, *Macromol. Rapid Commun.*, 2013, **34**, 471–484.
6 Y. Xu, S. Jin, H. Xu, A. Nagai and D. Jiang, *Chem. Soc. Rev.*, 2013, **42**, 8012–8031.
7 P. Kaur, J. T. Hupp and S. T. Nguyen, *ACS Catal.*, 2011, **1**, 819–835.
8 Y. Zhang and S. N. Riduan, *Chem. Soc. Rev.*, 2012, **41**, 2083–2094.
9 H. Xu, J. Gao and D. Jiang, *Nat. Chem.*, 2015, **7**, 905–912.
10 J. Jiang, Y. Li, X. Wu, J. Xiao, D. J. Adams and A. I. Cooper, *Macromolecules*, 2013, **46**, 8779–8783.
11 Y. Kou, Y. Xu, Z. Guo and D. Jiang, *Angew. Chem., Int. Ed.*, 2011, **50**, 8753–8757.
12 F. Xu, X. Chen, Z. Tang, D. Wu, R. Fu and D. Jiang, *Chem. Commun.*, 2014, **50**, 4788–4790.
13 C. Zhang, X. Yang, W. Ren, Y. Wang, F. Su and J. Jiang, *J. Power Sources*, 2016, **317**, 49–56.
14 X. Liu, Y. Xu and D. Jiang, *J. Am. Chem. Soc.*, 2012, **134**, 8738–8741.
15 Y. Zhang, A. Sigen, Y. Zou, X. Luo, Z. Li, H. Xia, X. Liu and Y. Mu, *J. Mater. Chem. A*, 2014, **2**, 13422–13430.
16 J. Jiang, A. Trewin, D. J. Adams and A. I. Cooper, *Chem. Sci.*, 2011, **2**, 1777–1781.
17 X. Wang, Y. Zhao, L. Wei, C. Zhang and J. Jiang, *J. Mater. Chem. A*, 2015, **3**, 21185–21193.
18 Y. Zhang, Y. Li, F. Wang, Y. Zhao, C. Zhang, X. Wang and J. Jiang, *Polymer*, 2014, **55**, 5746–5750.
19 S. Qiao, Z. Du, C. Yang, Y. Zhou, D. Zhu, J. Wang, X. Chen and R. Yang, *Polymer*, 2014, **55**, 1177–1182.
20 S. Qiao, Z. Du and R. Yang, *J. Mater. Chem. A*, 2014, **2**, 1877–1885.
21 X. Yang, M. Yu, Y. Zhao, C. Zhang, X. Wang and J. Jiang, *J. Mater. Chem. A*, 2014, **2**, 15139–15145.
22 C. Gu, D. Liu, W. Huang, J. Liu and R. Yang, *Polym. Chem.*, 2015, **6**, 7410–7417.
23 L. Pan, Q. Chen, J. Zhu, J. Yu, Y. He and B. Han, *Polym. Chem.*, 2015, **6**, 2478–2487.
24 W. Huang, C. Gu, T. Wang, C. Gu, S. Qiao and R. Yang, *RSC Adv.*, 2014, **4**, 62525–62531.
25 J. Huang, X. Zhou, A. Lamprou, F. Maya, F. Svec and S. R. Turner, *Chem. Mater.*, 2015, **27**, 7388–7394.
26 U. H. F. Bunz, K. Seehafer, F. L. Geyer, M. Bender, I. Braun, E. Smarsly and J. Freudenberg, *Macromol. Rapid Commun.*, 2014, **35**, 1466–1496.
27 W. Lu, Z. Wei, D. Yuan, J. Tian, S. Fordham and H. Zhou, *Chem. Mater.*, 2014, **26**, 4589–4597.
28 J. Chun, J. H. Park, J. Kim, S. M. Lee, H. J. Kim and S. U. Son, *Chem. Mater.*, 2012, **24**, 3458–3463.
29 L. Monnereau, T. Muller, M. Lang and S. Brase, *Chem. Commun.*, 2016, **52**, 571–574.
30 W. Song, X. Xu, Q. Chen, Z. Zhuang and X. Bu, *Polym. Chem.*, 2013, **4**, 4690–4696.
31 H. A. Patel, F. Karadas, J. Byun, J. Park, E. Deniz, A. Canlier, Y. Jung, M. Atilhan and C. T. Yavuz, *Adv. Funct. Mater.*, 2013, **23**, 2270–2276.
32 A. Karmakar, A. Kumar, A. K. Chaudhari, P. Samanta, A. V. Desai, R. Krishna and S. K. Ghosh, *Chem.–Eur. J.*, 2016, **22**, 4931–4937.
33 S. Altarawneh, T. Islamoglu, A. K. Sekizkardes and H. M. El-Kaderi, *Environ. Sci. Technol.*, 2015, **49**, 4715–4723.
34 V. Neti, J. Wang, S. Deng and L. Echegoyen, *RSC Adv.*, 2015, **5**, 10960–10963.
35 H. A. Patel, S. H. Je, J. Park, D. P. Chen, Y. Jung, C. T. Yavuz and A. Coskun, *Nat. Commun.*, 2013, **4**, 1357.
36 P. Arab, M. G. Rabbani, A. K. Sekizkardes, T. Islamoglu and H. M. El-Kaderi, *Chem. Mater.*, 2014, **26**, 1385–1392.
37 H. A. Patel, S. H. Je, J. Park, Y. Jung, A. Coskun and C. T. Yavuz, *Chem.–Eur. J.*, 2014, **20**, 772–780.
38 A. I. Cooper, *Adv. Mater.*, 2009, **21**, 1291–1295.
39 M. Grigoras and L. Stafie, *High Perform. Polym.*, 2009, **21**, 304–314.
40 J. Zeitouny, C. Aurisicchio, D. Bonifazi, R. De Zorzi, S. Geremia, M. Bonini, C. A. Palma, P. Samori, A. Listorti, A. Belbakra and N. Armaroli, *J. Mater. Chem.*, 2009, **19**, 4715–4724.
41 H. Ma, H. Ren, X. Zou, S. Meng, F. Sun and G. Zhu, *Polym. Chem.*, 2014, **5**, 144–152.
42 R. Yuan, H. Ren, Z. Yan, A. Wang and G. Zhu, *Polym. Chem.*, 2014, **5**, 2266–2272.
43 Z. Yan, H. Ren, H. Ma, R. Yuan, Y. Yuan, X. Zou, F. Sun and G. Zhu, *Microporous Mesoporous Mater.*, 2013, **173**, 92–98.
44 M. Cha, Y. Lim and J. Chang, *J. Polym. Sci., Part A: Polym. Chem.*, 2015, **53**, 2336–2342.

45 M. Trunk, A. Herrmann, H. Bildirir, A. Yassin, J. Schmidt and A. Thomas, *Chem.–Eur. J.*, 2016, **22**, 7179–7183.

46 H. Ma, H. Ren, X. Zou, F. Sun, Z. Yan, K. Cai, D. Wang and G. Zhu, *J. Mater. Chem. A*, 2013, **1**, 752–758.

47 W. Lu, D. Yuan, D. Zhao, C. I. Schilling, O. Plietzsch, T. Muller, S. Brase, J. Guenther, J. Blumel, R. Krishna, Z. Li and H. Zhou, *Chem. Mater.*, 2010, **22**, 5964–5972.

48 X. Jing, D. Zou, P. Cui, H. Ren and G. Zhu, *J. Mater. Chem. A*, 2013, **1**, 13926–13931.

49 S. Ren, R. Dawson, A. Laybourn, J. Jiang, Y. Khimyak, D. J. Adams and A. I. Cooper, *Polym. Chem.*, 2012, **3**, 928–934.

50 C. Zhang, X. Yang, Y. Zhao, X. Wang, M. Yu and J. Jiang, *Polymer*, 2015, **61**, 36–41.

51 Z. Yang, Y. Zhao, H. Zhang, B. Yu, Z. Ma, G. Ji and Z. Liu, *Chem. Commun.*, 2014, **50**, 13910–13913.

52 C. M. Thompson, G. T. McCandless, S. N. Wijenayake, O. Alfarawati, M. Jahangiri, A. Kokash, Z. Tran and R. A. Smaldone, *Macromolecules*, 2014, **47**, 8645–8652.

53 Y. Zhu, H. Long and W. Zhang, *Chem. Mater.*, 2013, **25**, 1630–1635.

54 M. Zhang, Z. Perry, J. Park and H. Zhou, *Polymer*, 2014, **55**, 335–339.

55 Q. Chen, M. Luo, P. Hammershoj, D. Zhou, Y. Han, B. W. Laursen, C. Yan and B. Han, *J. Am. Chem. Soc.*, 2012, **134**, 6084–6087.

56 P. Puthiaraj and W. Ahn, *Ind. Eng. Chem. Res.*, 2016, **55**, 7917–7923.

57 Q. Ma, B. Yang and J. Li, *RSC Adv.*, 2015, **5**, 64163–64169.

58 P. Puthiaraj, S. Kim and W. Ahn, *Chem. Eng. J.*, 2016, **283**, 184–192.

59 F. Jiang, J. Sun, R. Yang, S. Qiao, Z. An, J. Huang, H. Mao, G. Chen and Y. Ren, *New J. Chem.*, 2016, **40**, 4969–4973.

60 X. Zhang, J. Lu and J. Zhang, *Chem. Mater.*, 2014, **26**, 4023–4029.

61 T. Ratvijitvech, R. Dawson, A. Laybourn, Y. Z. Khimyak, D. J. Adams and A. I. Cooper, *Polymer*, 2014, **55**, 321–325.

62 A. Bhunia, I. Boldog, A. Moller and C. Janiak, *J. Mater. Chem. A*, 2013, **1**, 14990–14999.

63 X. Yang, S. Yao, M. Yu and J. Jiang, *Macromol. Rapid Commun.*, 2014, **35**, 834–839.

64 K. Sumida, D. L. Rogow, J. A. Mason, T. M. McDonald, E. D. Bloch, Z. R. Herm, T. Bae and J. R. Long, *Chem. Rev.*, 2012, **112**, 724–781.

65 C. Xu and N. Hedin, *J. Mater. Chem. A*, 2013, **1**, 3406–3414.